AIAA JOURNAL
Vol. 38, No. 3, March 2000

Investigation of Nonlinear Eddy-Viscosity Turbulence Models in Shock/Boundary-Layer Interaction

G. Barakos* and D. Drikakis†
UMIST, Manchester, England M60 1QD, United Kingdom

Validation of nonlinear two- and three-equation, eddy-viscosity turbulence models (NLEVM) in transonic flows featuring shock/boundary-layer interaction and separation is presented. The accuracy of the models is assessed against experimental results for two transonic flows over bump geometries. Moreover, the accuracy and efficiency of NLEVMs is also assessed in contrast to numerical predictions obtained by a variety of other models employed in this study. These include two linear eddy-viscosity k–ϵ models, the k–ω shear-stress transport model, and a nonlinear version of the k–ω model. Discretization of the mean flow and turbulence transport equations is obtained by a characteristics-based scheme (Riemann solver) in conjunction with an implicit unfactored method. The study shows that NLEVMs improve the numerical predictions in shock/boundary-layer interaction, compared to the linear models, but they require longer computing times.

Nomenclature

A	= Lumley's flatness parameter, $\equiv 1 - \frac{9}{8}(A_2 - A_3)$
A_2	= second invariant of Reynolds-stress anisotropy, $\equiv \alpha_{ij}\alpha_{ij}$
A_3	= third invariant of Reynolds-stress anisotropy, $\equiv \alpha_{ik}\alpha_{kj}\alpha_{ji}$
c	= bump length
c_p	= specific heat capacity at constant pressure
c_v	= specific heat capacity at constant volume
E, G, E_v, G_v	= inviscid and viscous fluxes, in curvilinear coordinates
$\tilde{E}, \tilde{G}, \tilde{E}_v, \tilde{G}_v$	= inviscid and viscous fluxes, in Cartesian coordinates
e	= total energy of the fluid per unit volume
H	= source term
H_A	= contribution to the source term originating from the axisymmetric formulation of the governing equations
J	= Jacobian of transformation from Cartesian to curvilinear coordinates
k	= turbulent kinetic energy, $\overline{u_i'u_i'}/2$
P_{ij}	= turbulence production $P_{ij} = -\rho\overline{u_k'u_i'}(\partial u_j/\partial x_k) - \rho\overline{u_k'u_j'}(\partial u_i/\partial x_k)$
Pr	= Prandtl number, $\rho\mu c_p/k$
Pr_t	= turbulent Prandtl number, $\rho\mu_t c_p/k$
p	= pressure
p_0	= reservoir pressure for Délery's case
p_∞	= reference pressure for case 8611
$\dot{q}_i, \dot{q}_{li}, \dot{q}_{ti}$	= total, molecular, and turbulent heat flux rates in the x_i coordinate direction
R	= ideal gas law constant
$\tilde{R}_t$	= near-wall Reynolds number, $\rho k^2/\mu\tilde{\epsilon}$
S	= strain invariant, $\equiv \sqrt{(S_{ij}S_{ij}/2)}$
S_{ij}	= strain tensor, $\equiv \partial u_i/\partial x_j + \partial u_j/\partial x_i$
S_k, S_ϕ	= contributions to the source term $\tilde{H}$ originating from the transport equations of the turbulence model
T	= temperature
T_0	= reservoir temperature for Délery's case
t	= time
u_i	= mean velocity component in the x_i direction $(i = 1, 2)$
u_τ	= friction velocity
x_i	= Cartesian coordinates $(i = 1, 2; x = x_1; z = x_2)$
y	= distance from solid boundary
y^+	= wall distance, $y\rho u_\tau/\mu$
α_{ij}	= Reynolds-stress anisotropy, $\equiv \overline{u_i'u_j'}/k - \frac{2}{3}\delta_{ij}$
γ	= ratio of specific heats, $\equiv c_p/c_v$
δ	= boundary-layer thickness
δ_{ij}	= Kronecker delta
δ^*	= displacement thickness of boundary layer
ϵ	= dissipation rate of k
$\tilde{\epsilon}$	= isotropic dissipation rate of k, $\equiv \epsilon - \hat{\epsilon}$, $\hat{\epsilon} \equiv 2(\mu/\rho)(\partial\sqrt{k}/\partial x_j)^2$
ϵ_{ij}	= dissipation rate of Reynolds-stress components
κ	= thermal conductivity
μ	= coefficient of dynamic viscosity
μ_T	= eddy viscosity
ξ, ζ	= curvilinear coordinates
ρ	= density
$-\rho\overline{u_i'u_j'}$	= Reynolds-stress tensor
τ	= time in the curvilinear coordinate system
τ_{ij}	= total stress tensor
τ_{lij}	= molecular stress tensor
τ_{tij}	= turbulent Reynolds-stress tensor
ϕ	= scalar variable
ϕ_{ij}	= pressure-strain term in the A_2 equation
ϕ_{ij}^w	= wall-reflection term of ϕ_{ij}
ϕ_{ij}^1	= return-to-isotropy fragment in pressure-strain term in the A_2 equation
ϕ_{ij}^2	= rapid fragment in pressure-strain term in the A_2 equation
Ω	= vorticity invariant, $\equiv \sqrt{(\Omega_{ij}\Omega_{ij}/2)}$
Ω_{ij}	= vorticity tensor, $\equiv \partial u_i/\partial x_j - \partial u_j/\partial x_i$
ω	= specific turbulent dissipation rate, turbulent frequency, $\equiv \epsilon/k$

Received 19 March 1998; revision received 15 August 1999; accepted for publication 23 August 1999.

*Research Associate, P.O. Box 88, Mechanical Engineering Department.
†Lecturer, Mechanical Engineering Department; currently Reader (Associate Professor) in CFD, Queen Mary & Westfield College, University of London, Department of Engineering, London, England E1 4NS, United Kingdom. Senior Member AIAA.

I. Introduction

SHOCK/BOUNDARY-LAYER interaction appears in many aeronautical applications such as flows in compressor passages and around turbomachinery blades and external flows over aircraft wings and helicopter blades. The aerodynamic performance in these applications depends strongly on the location and strength of the shocks, as well as on the flow separation induced by the

shock/boundary-layer interaction. Accurate prediction of the preceding flow phenomena is of primary technological importance, and their simulation remains a challenging problem because of the complex physics involved.

In the past, the phenomenon of turbulent shock/boundary-layer interaction has been the subject of extensive experimental and numerical investigations. The experiments in Refs. 1–5 have been used extensively in computational fluid dynamics (CFD) validation studies of turbulence models. Past research has revealed that the accuracy of numerical calculations is mainly dictated by the accuracy of the turbulence model. Experience using zero-equation turbulence models[6] has shown that these models do not provide satisfactory results, especially when flow separation is present. Linear eddy-viscosity models assume an explicit algebraic relationship between Reynolds stresses and mean strain, known as the Boussinesq approximation. These models provide satisfactory results for attached, fully developed turbulent boundary layers with weak pressure gradients and are also relatively easy to implement into CFD codes. However, the predictions deteriorate when all components of the Reynolds-stress tensor become dynamically significant. Linear low-Reynolds two-equation models seem to offer the best balance between accuracy and computational cost, but because of the employed Boussinesq approximation of the Reynolds-stress tensor, they are not able to capture effects arising from normal-stress anisotropy. Second-moment closures offer a more exact representation of the Reynolds stresses but require more computing resources and careful numerical implementation for obtaining stable numerical solutions. Reynolds-stress models have been used in the past to investigate shock/boundary-layer interaction.[7,8] These studies showed that in certain cases second-moment closures provide better results than linear models, but in other cases the results are inconclusive.

The objective behind the development and validation of nonlinear eddy-viscosity turbulence models (NLEVMs) is to introduce closures that incorporate key features of the Reynolds-stress models but which, however, require computational effort comparable to linear two-equation eddy-viscosity models. At present, nonlinear models seem to be one of the alternative routes for advanced modeling of turbulence beyond the linear eddy-viscosity models. For nonlinear models the eddy viscosity μ_T is still obtained by an algebraic relation, which involves the turbulent kinetic energy k and turbulent dissipation ϵ or dissipation rate ω, but the calculation of the Reynolds-stress components involves the quadratic and cubic products of the strain and vorticity tensors. Nonlinear models are still being refined and validated for steady flows, mainly two dimensional and incompressible,[9–11] whereas limited experience has been acquired from applications to compressible flows.[12,13]

The aim of the present study is to validate two- and three-equation NLEVMs in transonic flows with shock/boundary-layer interaction. The specific objectives of this paper are 1) to validate the accuracy of the cubic NLEVM by Craft et al.[10] as well as the three-equation cubic NLEVM by Suga[14] against experimental results for transonic flows over bump geometries[1–5]; 2) to compare the NLEVM predictions with those obtained by a variety of other models, including the Launder–Sharma[15] and Nagano–Kim[16] linear k–ϵ EVMs, the two-equation k–ω shear-stress transport (SST) model by Menter,[17,18] and the nonlinear k–ω model by Sofialidis and Prinos[19]; and 3) to evaluate the efficiency of the models by comparing the CPU time of the NLEVM and linear eddy-viscosity model (EVM), when these are implemented into the same numerical framework, namely in conjunction with the same discretization scheme and iterative solver.

The paper is organized as follows: Sec. II presents the governing equations and numerical method, Sec. III summarizes the NLEVM formulations employed in this study, Sec. IV presents and discusses the results, and finally, Sec. V contains conclusions from the present study.

II. Mathematical Model

The time-averaged Navier–Stokes equations for a compressible fluid are employed:

$$\frac{\partial \rho}{\partial t} + \frac{\partial}{\partial x_i}(\rho u_i) = 0 \tag{1}$$

$$\frac{\partial \rho u_i}{\partial t} + \frac{\partial}{\partial x_i}(\rho u_i u_j + p\delta_{ij} - \tau_{ij}) = 0 \tag{2}$$

$$\frac{\partial e}{\partial t} + \frac{\partial}{\partial x_i}[u_i(e + p) - u_i \tau_{ij} + \dot{q}_i] = 0 \tag{3}$$

In the preceding equations the ideal gas equation of state ($p = \rho RT$) is used to calculate the pressure p, and τ_{ij} denotes the sum of the laminar and Reynolds-stress tensors.

To close the preceding system of equations, the definitions of the turbulent Reynolds stresses and heat fluxes $\dot{q}_i$ as functions of the mean flow quantities is required. For the linear EVM the stress tensor is defined, according to the Boussinesq approximation, to be proportional to the mean strain-rate tensor, with the factor of proportionality being the eddy viscosity μ_T. The eddy viscosity is modeled in terms of the turbulent kinetic energy and a turbulence scale variable. The total stresses and heat fluxes for the case of linear EVMs are calculated as follows:

$$\tau_{ij} = \tau_{\mathrm{lij}} + \tau_{\mathrm{tij}} \tag{4}$$

$$\tau_{\mathrm{lij}} = \mu(S_{ij} - S_{nn}\delta_{ij}/3) \tag{5}$$

$$\tau_{\mathrm{tij}} = \mu_T(S_{ij} - S_{nn}\delta_{ij}/3) - 2\rho k\delta_{ij}/3 \tag{6}$$

The heat-flux rates are modeled according to Fourier's law as

$$\dot{q}_i = \dot{q}_{li} + \dot{q}_{ti} = -\left(\frac{\mu}{Pr} + \frac{\mu_T}{Pr_T}\right)\frac{\partial T}{\partial x_i} \tag{7}$$

Different formulations are used for the NLEVM, and these are presented in Sec. III.

The compressible Navier–Stokes equations in conjunction with a two-equation turbulence model can be written in a matrix form and for a curvilinear (τ, ξ, ζ) coordinate system as

$$\frac{\partial U}{\partial \tau} + \frac{\partial E}{\partial \xi} + \frac{\partial G}{\partial \zeta} = \frac{\partial E_v}{\partial \xi} + \frac{\partial G_v}{\partial \zeta} + H \tag{8}$$

where

$$U = J\tilde{U}, \qquad \tilde{U} = (\rho, \rho u, \rho w, e, \rho k, \rho\phi)^T, \qquad H = J\tilde{H} \tag{9}$$

and ϕ may be one of the following: the turbulent dissipation rate ϵ, the isotropic part of the turbulent dissipation rate $\tilde{\epsilon}$, or the specific turbulent dissipation rate ω.

The matrix $\tilde{H}$ has nonzero entries for the source terms of the turbulence-model equations as well as for terms from the axisymmetric formulation:

$$\tilde{H} = (0, 0, 0, 0, S_k, S_\phi)^T + H_A \tag{10}$$

where the first matrix corresponds to the turbulence model source terms and the second one (H_A) holds sources from the axisymmetric formulation.[20]

The inviscid E, G, and viscous E_v, G_v fluxes are written in curvilinear coordinates as functions of their corresponding Cartesian counterparts, e.g.,

$$E = J(\tilde{E}\xi_x + \tilde{G}\xi_z) \tag{11}$$

Because the aim of the present study is the validation of turbulence models, a very brief description of the numerical method employed for the solution of the governing equations is given here. A detailed description can be found in Ref. 21. A third-order upwind scheme in conjunction with a characteristics-based flux averaging (Riemann solver) is used to calculate the inviscid fluxes at the cell faces of the computational volumes.[22–24] Limiters based on the squares of second-order pressure derivatives have been used for detecting shock waves and contact discontinuities, whereas central differences are used for discretizing the viscous terms. Both explicit and implicit schemes have been implemented into the CFD

code.[21] In the present study the implicit version of the method has been employed according to which the six or seven equations—in the case of a three-equation turbulence model—are simultaneously solved by an implicit-unfactored method, which combines Newton subiterations and Gauss–Seidel relaxation.

III. Turbulence Modeling

The idea behind NLEVMs can be found in the paper by Pope,[25] and later Speziale[26] and Speziale and Ngo[27] demonstrated the ability of nonlinear models to capture secondary flows in ducts. Furthermore, Rubinstein and Barton[28] developed a nonlinear model based on the renormalization group theory,[29,30] and Shih et al.[31] developed a realizable nonlinear algebraic-stress model. Other attempts to use advanced turbulence models in aerodynamic flows can be found in the works by Gatski,[12] Jiang et al.,[32] Lien and Leschziner,[33] and Barakos and Drikakis.[13]

Craft et al.[9] and Suga[14] developed low-Reynolds, cubic NLEVMs and applied them to incompressible flows. Their studies indicate that these models are able to give results close to the ones obtained by second-moment closures. Both models employ a cubic expansion of the Reynolds-stress tensor in terms of the strain and vorticity invariants in contrast to the quadratic expansion employed by Speziale and Ngo.[27] Although the preceding models originate from the linear k–ϵ EVM, the development of nonlinear k–ω EVM has also been made by other authors.[19]

The interest of the scientific community in NLEVM is justified by the promising capabilities of these models to capture effects arising from Reynolds-stress anisotropy in complex flow conditions. It also appears that they are more economic in terms of computing resources compared to the Reynolds-stress transport models. However, the level of complexity of NLEVM can also be high, and their numerical implementation may become cumbersome.

In the present work the capabilities of NLEVMs for predicting shock/boundary-layer interaction are investigated against experimental data and results obtained by linear EVMs. Therefore, the following models have been employed: the Nagano–Kim k–ϵ (Ref. 16), the Launder–Sharma (LS) k–ϵ (Ref. 15), the SST k–ω by Menter (SST),[17,18] the cubic nonlinear k–ϵ model by Craft et al.[9] (NL k–ϵ), the cubic nonlinear k–ϵ–A_2 model by Suga[14] (NL k–ϵ–A_2), and the cubic nonlinear k–ω model by Sofialidis and Prinos[19] (NL k–ω). The nonlinear models considered here have been calibrated in the past against experimental data for incompressible flows, and no change has been introduced here regarding models, coefficients, and source terms.

A description of the nonlinear models is given in the next paragraphs, whereas the description of the linear k–ϵ models as well as of the SST k–ω model can be found in the corresponding references.

A. Cubic Nonlinear k–ϵ EVM

For the k–ϵ NLEVM by Craft et al.,[10] the transport equations for k and $\tilde{\epsilon}$ are

$$\frac{\partial \rho k}{\partial t} + \frac{\partial \rho u_i k}{\partial x_i} = d_k + P_k - \rho\epsilon \tag{12}$$

$$\frac{\partial \rho \tilde{\epsilon}}{\partial t} + \frac{\partial \rho u_i \tilde{\epsilon}}{\partial x_i} = d_{\tilde{\epsilon}} + c_{\epsilon 1} P_k \frac{\tilde{\epsilon}}{k} - c_{\epsilon 2} \frac{\rho \tilde{\epsilon}^2}{k} + P_{\epsilon 3} + S_\epsilon \tag{13}$$

In the preceding equation the summation stands only for the i index, and the diffusion terms d_k and $d_{\tilde{\epsilon}}$ are written as

$$d_k = \frac{\partial}{\partial x_l}\left(\left(\mu + \frac{\mu_T}{1.0}\right)\frac{\partial k}{\partial x_l}\right), \qquad d_{\tilde{\epsilon}} = \frac{\partial}{\partial x_l}\left(\left(\mu + \frac{\mu_T}{1.3}\right)\frac{\partial \tilde{\epsilon}}{\partial x_l}\right) \tag{14}$$

The production term P_k and the near-wall term $P_{\epsilon 3}$ are

$$P_k = \rho c_\mu f_\mu \tilde{\epsilon} \tilde{S} \tilde{\Omega} \tag{15}$$

$$P_{\epsilon 3} = 0.0022 \frac{\tilde{S}\mu_T k^2}{\tilde{\epsilon}}\left(\frac{\partial^2 u_i}{\partial x_k \partial x_l}\right)^2, \qquad \tilde{R}_t \le 250 \tag{16}$$

$$P_{\epsilon 3} = 0, \qquad \tilde{R}_t \ge 250 \tag{17}$$

and the coefficients $c_{\epsilon i}$ of the dissipation equation have the values

$$c_{\epsilon 1} = 1.44, \qquad c_{\epsilon 2} = 1.92\left[1 - 0.3\exp\left(-\tilde{R}_t^2\right)\right] \tag{18}$$

$\tilde{S}$ and $\tilde{\Omega}$ are the normalized invariants of the strain and vorticity tensors S and Ω, respectively:

$$\tilde{S} \equiv \frac{k}{\tilde{\epsilon}}\sqrt{\frac{S'_{ij}S'_{ij}}{2}}, \qquad S'_{ij} \equiv S_{ij} - \frac{1}{3}\delta_{ij}S_{kk}, \qquad \tilde{\Omega} \equiv \frac{k}{\tilde{\epsilon}}\sqrt{\frac{\Omega_{ij}\Omega_{ij}}{2}} \tag{19}$$

Finally, the so-called Yap's correction S_ϵ is

$$S_\epsilon = \max\left[0.83\left(\frac{k^{\frac{3}{2}}}{2.5\tilde{\epsilon}y} - 1\right)\left(\frac{k^{\frac{3}{2}}}{2.5\tilde{\epsilon}y}\right)^2 \frac{\rho\tilde{\epsilon}^2}{k}, 0\right] \tag{20}$$

where y is the distance from the wall.

Because of the marginal improvement provided in most flow cases by quadratic nonlinear expansions of the anisotropy Reynolds-stress tensor a_{ij}, a cubic expansion has been suggested by Craft et al.[10]:

$$\begin{aligned} a_{ij} = {} & -\frac{\mu_T}{\rho k}S'_{ij} + c_1\frac{\mu_T}{\rho\tilde{\epsilon}}\left(S'_{ik}S'_{kj} - \frac{1}{3}S'_{kl}S'_{kl}\delta_{ij}\right) \\ & + c_2\frac{\mu_T}{\rho\tilde{\epsilon}}(\Omega_{ik}S'_{kj} + \Omega_{jk}S'_{ki}) + c_3\frac{\mu_T}{\rho\tilde{\epsilon}}\left(\Omega_{ik}\Omega_{jk} - \frac{1}{3}\Omega_{lk}\Omega_{lk}\delta_{ij}\right) \\ & + c_4\frac{\mu_T k}{\rho\tilde{\epsilon}^2}(S'_{ki}\Omega_{lj} + S'_{kj}\Omega_{li})S'_{kl} + c_5\frac{\mu_T k}{\rho\tilde{\epsilon}^2}\left(\Omega_{il}\Omega_{lm}S'_{mj}\right. \\ & \left. + S'_{il}\Omega_{lm}\Omega_{mj} - \frac{2}{3}S'_{lm}\Omega_{mn}\Omega_{nl}\delta_{ij}\right) + c_6\frac{\mu_T k}{\rho\tilde{\epsilon}^2}S'_{ij}(S'_{kl}S'_{kl} - \Omega_{kl}\Omega_{kl}) \end{aligned} \tag{21}$$

The preceding is, subsequently, used to calculate the components of the Reynolds-stress tensor.

The coefficients c_i appearing in Eq. (21) take the values

$$c_1 = -0.1, \qquad c_2 = 0.1, \qquad c_3 = 0.26$$
$$c_4 = -10c_\mu^2, \qquad c_5 = 0, \qquad c_6 = -5c_\mu^2 \tag{22}$$

The eddy viscosity is calculated by

$$\mu_T = c_\mu \rho f_\mu (k^2/\tilde{\epsilon}) \tag{23}$$

where

$$c_\mu = \frac{0.3\{1 - \exp[-0.36\exp(0.75\eta)]\}}{1 + 0.35\eta^{1.5}} \tag{24}$$

$$f_\mu = 1 - \exp\left[-(\tilde{R}_t/90)^{\frac{1}{2}} - (\tilde{R}_t/400)^2\right] \tag{25}$$

$$\eta = \max(\tilde{S}, \tilde{\Omega}) \tag{26}$$

Such functional form of c_μ has been found to be beneficial in flows far from equilibrium and has also been employed in the work by Liou and Shih[34] for shock/boundary-layer interaction problems.

B. Cubic Nonlinear k–ϵ–A_2 EVM

To obtain a better representation of the turbulence anisotropy, the three-equation model by Suga[14] uses an additional transport equation for the second invariant A_2 of the Reynolds-stress anisotropy tensor. As reported in Refs. 14 and 35, inclusion of the third equation makes the numerical results comparable to those obtained by differential Reynolds-stress models. In addition, the CPU time is slightly increased, while the model becomes free of the wall-distance.

The extra equation for the invariant A_2 of the turbulence anisotropy tensor a_{ij} is written as

$$\frac{\mathrm{D}A_2}{\mathrm{D}t} = dA_2 - 2\frac{A_2}{k}P_k + 2\frac{a_{ij}}{k}P_{ij} + 2\frac{a_{ij}}{k}\phi_{ij} + 2\frac{A_2}{k}\epsilon - 2\frac{a_{ij}}{k}\epsilon_{ij} \tag{27}$$

where the diffusive part dA_2 is modeled as

$$dA_2 = \frac{\partial}{\partial x_k}\left(\left(\nu\delta_{kl} + 0.22 f_g \overline{u_k' u_l'}\frac{k}{\tilde{\epsilon}}\right)\frac{\partial A_2}{\partial x_l}\right) \tag{28}$$

and the pressure-strain term ϕ_{ij} is

$$\phi_{ij} = \phi_{ij1} + \phi_{ij2} + \phi_{ij}^{w} \tag{29}$$

$$\phi_{ij1} = -\tilde{c}_1\epsilon\left[a_{ij} + c_1'\left(a_{ik}a_{jk} - \tfrac{1}{3}A_2\delta_{ij}\right)\right] - \sqrt{A^*}\epsilon a_{ij} \tag{30}$$

$$\phi_{ij2} = -0.6\left(P_{ij} - \tfrac{1}{3}P_{kk}\delta_{ij}\right) + 0.3\epsilon a_{ij}(P_{kk}/\epsilon) \tag{31}$$

$$\begin{aligned}\phi_{ijw} = {} & -c_{2w}\frac{\partial u_l}{\partial x_m}\overline{u_l' u_m'}\left(\frac{\partial l_f}{\partial x_q}\frac{\partial l_f}{\partial x_q}\delta_{ij} - 3\frac{\partial l_f}{\partial x_i}\frac{\partial l_f}{\partial x_j}\right) \\ & - c_{2w}' k\left(a_{lm}\frac{\partial u_k}{\partial x_m}\frac{\partial l_f}{\partial x_l}\frac{\partial l_f}{\partial x_k}\delta_{ij} - \frac{3}{2}a_{lm}\frac{\partial u_i}{\partial x_m}\frac{\partial l_f}{\partial x_l}\frac{\partial l_f}{\partial x_j}\right. \\ & \left. - \frac{3}{2}a_{lm}\frac{\partial u_j}{\partial x_m}\frac{\partial l_f}{\partial x_l}\frac{\partial l_f}{\partial x_i}\right) + c_{2w}'' k\frac{\partial u_l}{\partial x_m}\frac{\partial l_f}{\partial x_l}\frac{\partial l_f}{\partial x_m} \\ & \times\left(\frac{\partial l_f}{\partial x_i}\frac{\partial l_f}{\partial x_j} - \frac{1}{3}\frac{\partial l_f}{\partial x_q}\frac{\partial l_f}{\partial x_q}\delta_{ij}\right)\end{aligned} \tag{32}$$

The dissipation tensor ϵ_{ij} is modeled as

$$\epsilon_{ij} = f_\epsilon\epsilon_{ij}^* + (1 - f_\epsilon)\tfrac{2}{3}\delta_{ij}\epsilon \tag{33}$$

$$\begin{aligned}\epsilon_{ij}^* = {} & \left(2\frac{\mu}{\rho}f_\epsilon^*\frac{\partial\sqrt{k}}{\partial x_m}\left(\frac{\partial\sqrt{k}}{\partial x_i}\frac{\overline{u_j' u_m'}}{k} + \frac{\partial\sqrt{k}}{\partial x_j}\frac{\overline{u_i' u_m'}}{k}\right)\right. \\ & \left. + 2\frac{\mu}{\rho}f_\epsilon^*\frac{\partial\sqrt{k}}{\partial x_k}\frac{\partial\sqrt{k}}{\partial x_m}\frac{\overline{u_k' u_m'}}{k}\delta_{ij} + \frac{\overline{u_i' u_j'}}{k}\epsilon\right) \\ & \Bigg/\left(1 + \frac{5\mu f_\epsilon^*}{\rho\epsilon}\frac{\partial\sqrt{k}}{\partial x_k}\frac{\partial\sqrt{k}}{\partial x_m}\frac{\overline{u_k' u_m'}}{k}\right)\end{aligned} \tag{34}$$

The coefficients and functions for the A_2 transport equation are given by

$$\tilde{c}_1 = 3.1\min\left(\sqrt{A_2}, 0.5\right)\sqrt{A^*}f_\phi, \qquad c_1' = 1.2 \tag{35}$$

$$c_{2w} = 0.088A_2^2, \qquad c_{2w}' = 0.16A_2^2, \qquad c_{2w}'' = 1.2f_\phi A_2^2 \tag{36}$$

$$l_f = \frac{1 - \exp(-\tilde{R}_t/30)}{1 + 3.5A_2^2}\frac{k^{1.5}}{\epsilon}, \qquad f_\phi = 1 - \exp\left[-\left(\frac{\tilde{R}_t}{80}\right)^2\right] \tag{37}$$

$$f_A = \exp(-20A''^2) \tag{38}$$

$$f_\epsilon = 1 - f_\phi[1 - \exp(-20A^{*1.5})], \qquad f_\epsilon^* = 1 - \exp\left(\frac{-\tilde{R}_t}{1 + 2A_2^2}\right) \tag{39}$$

The effective values of A appearing in damping functions and coefficients of the transport equation are given next:

$$A^* = f_A A' + (1 - f_A)A'', \qquad A' = A\left(1 - \exp\left(\frac{-\tilde{R}_t^2}{1 + 24A_2}\right)\right) \tag{40}$$

$$A'' = \left\{1 - \frac{9}{8}\left[A_2 - A_3\left(\frac{A_2}{a_{ij}a_{ij}}\right)^{1.5}\right]\right\}\left\{1 - \exp\left[-\left(\frac{\tilde{R}_t}{10}\right)^2\right]\right\}\frac{\tilde{\epsilon}}{\epsilon} \tag{41}$$

This model uses the same expansion of the anisotropy tensor as the two-equation models; however the c_i coefficients are different. In addition, the effective values S_{ij}^* and Ω_{ij}^* of S_{ij}' and Ω_{ij}:

$$S_{ij}^* = r_\eta S_{ij}', \qquad \Omega_{ij}^* = r_\eta\Omega_{ij} \tag{42}$$

are used in the cubic expansion of α_{ij}. The modified closure coefficients are given by

$$c_1 = -0.05\frac{f_q}{f_\mu}, \qquad c_2 = 0.11\frac{f_q}{f_\mu}, \qquad c_3 = 0.21\frac{f_q\tilde{S}}{f_\mu(\tilde{S} + \tilde{\Omega})/2} \tag{43}$$

$$c_4 = -0.8f_c, \qquad c_5 = 0, \qquad c_6 = -0.5f_c \tag{44}$$

while c_μ is also modified as

$$c_\mu = \frac{0.667r_\eta\left\{1 - \exp\left[-0.415\exp\left(1.3\eta^{\frac{5}{6}}\right)\right]\right\}}{1 + 1.8\eta} \tag{45}$$

Additionally, all damping functions are now free of wall-distance dependencies, and these are listed next:

$$f_q = \frac{r_\eta}{(1 + 0.0086\eta^2)^{\frac{1}{2}}}, \qquad f_c = \frac{r_\eta^2}{1 + 0.45\eta^{2.5}} \tag{46}$$

$$f_\mu = \frac{1.1\sqrt{\tilde{\epsilon}/\epsilon}[1 - 0.8\exp(-\tilde{R}_t/30)]}{1 + 0.6A_2 + 0.2A_2^{3.5}} \tag{47}$$

$$\eta = \max(\tilde{S}, \tilde{\Omega})r_\eta \tag{48}$$

$$r_\eta = 1 + \left\{1 - \exp\left[-(A_2/0.5)^3\right]\right\}\left[1 + 4\sqrt{\exp(-\tilde{R}_t/20)}\right] \tag{49}$$

The structure of the transport equations for k and $\tilde{\epsilon}$ remains the same as for the two-equation NLEVM; however, the diffusion and source terms are different:

$$P_k = \rho c_\mu f_\mu\tilde{\epsilon}\tilde{S}\tilde{\Omega} \tag{50}$$

$$d_k = \frac{\partial}{\partial x_k}\left(\left(\mu\delta_{kl} + 0.22 f_g\overline{u_k' u_l'}\frac{\rho k}{\tilde{\epsilon}}\right)\frac{\partial k}{\partial x_l}\right) \tag{51}$$

$$d_{\tilde{\epsilon}} = \frac{\partial}{\partial x_k}\left(\left(\mu\delta_{kl} + 0.18 f_g\overline{u_k' u_l'}\frac{\rho k}{\tilde{\epsilon}}\right)\frac{\partial\tilde{\epsilon}}{\partial x_l}\right) \tag{52}$$

$$f_g = 5(\epsilon/\tilde{\epsilon})^{\frac{1}{2}} - 4(\epsilon/\tilde{\epsilon})^{\frac{1}{4}} \tag{53}$$

$$c_{\epsilon 1} = 1 + 0.15(1 - A^*) \tag{54}$$

$$c_{\epsilon 2} = 1.92\Bigg/\left[1 + 0.7\left(1 - \frac{1}{1 + \tilde{R}_t^{2|}\ 400}\right)\sqrt{A_2}\max(0.25, A^*)\right] \tag{55}$$

$$P_{\epsilon 3} = 1.2\frac{\mu\mu_T}{\rho}\frac{\partial^2 u_i}{\partial x_k\partial x_j}\frac{\partial^2 u_i}{\partial x_k\partial x_j} + 1\frac{\mu\mu_T}{k\rho}\frac{\partial k}{\partial x_k}\frac{\partial u_i}{\partial x_l}\frac{\partial^2 u_i}{\partial x_k\partial x_l} \tag{56}$$

$$\begin{aligned}S_\epsilon = {} & -\frac{\rho\tilde{\epsilon}\tilde{\epsilon}}{k}\exp\left(-\frac{\tilde{R}_t^2}{4}\right) + 35\left(\frac{\partial u_i}{\partial x_m}\frac{\partial l}{\partial x_l}\frac{\partial l}{\partial x_m}\right) \\ & \times\left(\frac{\partial u_p}{\partial x_q}\frac{\partial l}{\partial x_p}\frac{\partial l}{\partial x_q}\right)\frac{\rho k\tilde{\epsilon}}{\tilde{\epsilon}}\end{aligned} \tag{57}$$

where $l \equiv k^{1.5}/\epsilon$.

IV. Results

The bump geometry is one of the most broadly used configurations for validating turbulence models in shock/boundary-layer interaction. The simulation of flows over bump geometries has been the subject of various efforts such as the BRITE/EURAM EUROVAL project[36] and the AFOSR–HTTM–Stanford Conference,[37] as well as more recent studies, e.g., Ref. 38 (and references therein). Two transonic flow cases over bump geometries, involving

shock/boundary-layer interaction and separation, have been considered in this work. For both test cases surface pressure as well as laser Doppler velocimetry measurements are available, and, thus, it is possible to assess the accuracy of the models by comparing the velocity and turbulent shear-stress profiles at various positions.

For the first bump flow case considered here, identified as Case 8611 at the 1980 AFOSR–HTTM–Stanford conference, experimental data have been contributed by Johnson et al.[2] A schematic representation of the flow configuration is shown in Fig. 1a. A freestream is allowed to form a boundary layer around a cylinder placed in front of the bump. The leading edge of the bump is smooth, and at its origin the center of the coordinate system (i.e., $x = z = 0$) has been placed. The bump is assumed symmetric around the cylinder, and its length c has been used as the characteristic length of the problem. A detailed description of the bump geometry can be found in Ref. 1. Because the axisymmetric configuration provides a flow free of three-dimensional effects, the preceding case is considered as one of the very few two-dimensional cases available for validation of turbulence models in transonic flow conditions.[39,40] The working fluid is air at $M_\infty = 0.875$, and the Reynolds number per unit length is $Re/m = 13.6 \times 10^6/\text{m}$. The experimental data obtained at the NASA Ames Research Center transonic wind tunnel[2] revealed a shock over the bump at about $x/c = 0.63$ as well as separation of the boundary layer occurring between $x/c = 0.7$ and 1.1.

The second test case, identified as ONERA Case C, has been contributed by Délery at the 1980–81 Stanford Conference.[4,37] In Fig. 1b a schematic of the geometry is shown, and the exact description can be found in Refs. 4 and 37. For this case the inlet Mach number is 0.63. The flow is accelerated over the bump until a Mach number close to 1.4 is achieved. The value of the downstream pressure, which is controlled by an adjustable throat, results in a normal shock wave above the trailing edge of the bump. The pressure gradient induced by the shock is strong enough to create boundary-layer separation on the lower wall. Downstream of the separation point, the flow becomes again supersonic, and a second shock quasi-normal to the lower wall is formed. The two shocks join each other above the interaction zone and form a single normal shock that interacts with the boundary layer on the upper wall. The separation and reattachment points were found to be at $x = 0.260$ and 0.325 m, respectively, away from the leading edge of the bump. The reservoir conditions for this problem are $P_0 = 95{,}000\ \text{N/m}^2$ and $T_0 = 300$ K. A comparison between various calculations using different models and numerical schemes can be found in the work by Haase et al.[36]

At first, numerical simulations have been performed for the case 8611. For this case there are also recent results using various linear EVMs.[31,38] A computational grid with 160×80 cells has been employed. This was found to be adequate for obtaining grid-independent solutions, and the same has also been shown by Shih et al.[31] For this test case the linear k–ϵ model of Launder and Sharma[15] and the SST model of Menter,[18] as well as the two- and three-equation NLEVMs, were used.

Results for the separation bubble are presented in Figs. 2a and 2b by plotting the streamlines around the trailing edge. As can be seen, the size and shape of the separation bubble depends on the model employed. The NLEVM as well as the SST models tend to predict longer and thicker bubbles than the linear model. This can also be seen from the results in Table 1, if one looks at the predictions for the separation and reattachment positions. The results in Table 1 show that the linear SST k–ω and the nonlinear k–ϵ models provide the best predictions regarding the separation and reattachment positions. Yet, the value of the maximum Mach number is better predicted by the nonlinear models, whereas the results are inconclusive regarding the shock location. Moreover, the linear SST k–ω, the nonlinear

Table 1 Comparisons between model predictions and experimental data for the shock, separation, reattachment locations x/c, and maximum Mach number (case 8611)

Model	Shock location	Separation point	Reattachment point	Maximum Mach number
LS	0.61	0.78	1.08	1.29
SST	0.65	0.74	1.08	1.29
NL k–ϵ	0.66	0.74	1.07	1.30
NL k–ω	0.69	0.77	1.07	1.31
NL k–ϵ–A_2	0.59	0.79	1.05	1.31
Experimental[2]	0.63	0.70	1.10	1.32

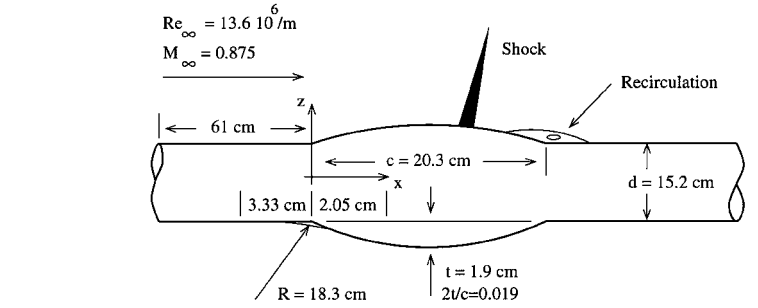

a) Case 8611

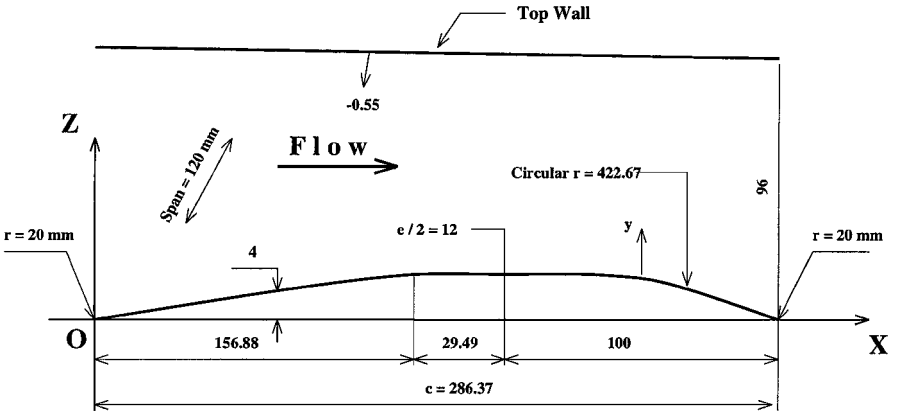

b) ONERA case C

Fig. 1 Schematic representation of the test cases.

Table 2 Boundary-layer properties using various turbulence models (case 8611)

Model	Maximum τ_{txz} (dimensionless)	Location (x/c) of maximum τ_{txz}	Maximum δ^*	Location (x/c) of maximum δ^*
LS	0.0075	1.067	1.29	1.001
SST	0.0101	0.990	1.24	1.003
NL k–ϵ	0.0093	0.987	1.32	1.003
NL k–ω	0.0107	0.932	1.20	1.003
NL k–ϵ–A_2	0.0114	1.059	1.21	1.003
Experimental[2]	0.019	1.15	1.2	1.02

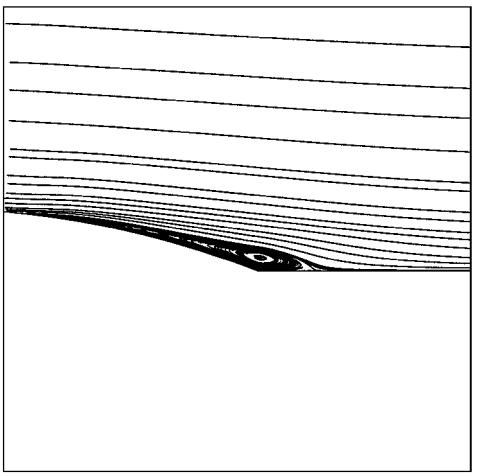

a) SST model

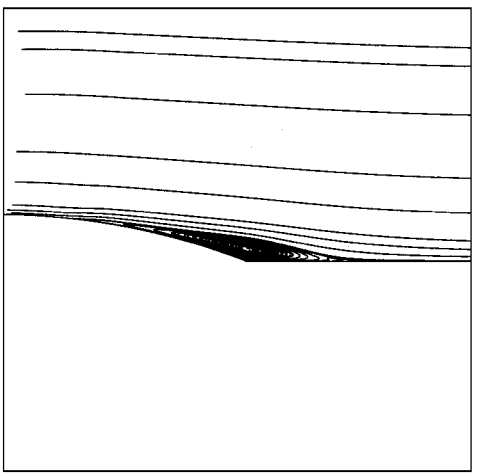

b) NL k–ϵ–A_2 model

Fig. 2 Prediction of the separated flow region for the case 8611.

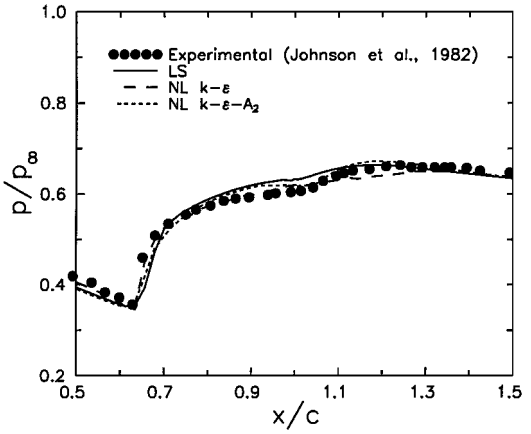

k–ϵ models

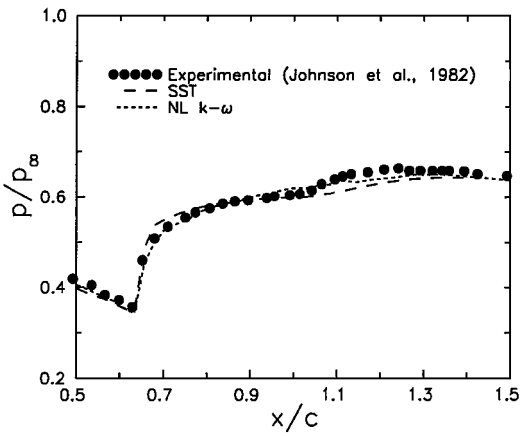

k–ω models

Fig. 3 Comparison between experimental data and numerical results for the surface pressure distribution over the axisymmetric bump (case 8611).

k–ϵ, and the nonlinear k–ω models predict the shock downstream of the experimentally indicated position, whereas the LS k–ϵ and nonlinear k–ϵ–A_2 models predict it upstream. All in all, the linear SST k–ω and the nonlinear k–ϵ models predict more accurately the shock location.

In Table 2 the numerically predicted boundary-layer values are compared with the measured ones. The boundary-layer separation depends on the balance between shear stress and pressure gradient. It is, thus, important to predict correctly the location and value of the maximum shear stress as well as the pressure distribution. The results in Table 2 show that all models underpredict the maximum value of the shear stress. The nonlinear k–ϵ–A_2 gives the best predictions both for the maximum shear stress and for the x/c location in which it appears. Moreover, the nonlinear k–ω and k–ϵ–A_2 models provide the best results for the maximum value of the boundary-layer thickness δ^*. All in all, the preceding two models seem to provide the best results for the boundary-layer quantities, at least for the present case.

In Fig. 3 the surface pressure distributions obtained using various models are shown. Larger differences between the models are presented close to the shock wave as well as downstream of it, where a pressure plateau is formed. The nonlinear k–ω, nonlinear k–ϵ, and the linear SST k–ω models give the best results downstream of the shock wave. The nonlinear k–ϵ–A_2 also provides reasonable results, but slightly overpredicts the pressure plateau compared to the preceding models. On the other hand, this model performs better downstream of the trailing edge.

Detailed comparisons between the various models predictions are also shown in Fig. 4 for the velocity and turbulent shear-stress profiles. The linear models give better results for the velocity profiles just after the separation point, upstream of the trailing edge. At $x/c = 1$ the best results are obtained by the nonlinear k–ϵ and the linear SST k–ω model. Concerning the turbulent shear-stress profiles, the results show that the nonlinear models provide, in general, larger values than the linear models. At the trailing edge $(x/c = 1)$ the nonlinear models provide better results than the linear ones. However, the results are rather inconclusive just downstream of the onset of separation $(x/c = 0.75)$, although the maximum shear-stress values obtained by the nonlinear models are closer to the experiment. At $x/c = 0.75$ the best results are provided by the nonlinear k–ϵ and SST k–ω models.

For the second test case (Fig. 1b) four turbulence models were compared: the Nagano–Kim[16] k–ϵ model, the SST[18] model, and the NLEVM k–ϵ and k–ϵ–A_2 models of Craft et al.[9,10] and Suga.[14] A grid with 121×121 cells was employed, and, as was also found in previous studies,[36] this grid size is sufficient for obtaining grid-independent solutions. The exit pressure is an important parameter for controlling the shock position, and the value of 60 Pa gives

correct shock positions both in computations with the linear and nonlinear models.

As can be seen from the pressure distribution on the lower wall (Fig. 5), the predictions by the linear and nonlinear models are in good agreement with the experimental data before the separation region. Most of the differences are encountered in the pressure plateau region, downstream of the shock wave where flow separation occurs. The nonlinear models capture marginally better the pressure distribution, and, to a certain degree, this is because of the functional form of the c_μ coefficient.

In Fig. 6 the numerical predictions for the velocity and turbulent shear stress are compared with the experimental data. As shown from the velocity profiles, better predictions in the separation region are obtained by the nonlinear k–ϵ model but with little difference from the results of the k–ϵ–A_2 model. The preceding observation is also supported by the values of the separation and reattachment points, as well as the maximum Mach number, reported in Table 3.

The shear-stress profiles presented in Fig. 6 show that all linear models underestimate the magnitude of the turbulent shear stress, whereas the nonlinear ones give slightly better predictions. The k–ϵ–A_2 model was expected to give better results for the Reynolds stresses because it is supposed to be sensitive to the anisotropy of the turbulent flow. Examining the experimental data by Délery, one can see that the measurements indicate a magnitude of u' velocities about 16 times higher than w'. As reported in the work by Benay et al.,[41] such an anisotropy is mainly caused by oscillations of the shock wave. However, the present simulations are for steady-state flow, and, therefore, any anisotropy induced by inherent unsteady effects cannot be captured.

The iso-Mach lines for the linear Nagano–Kim EVM and the nonlinear k–ϵ–A_2 EVM are shown in Figs. 7 and 8, respectively. The nonlinear model predicts better the strength of the λ-shock structure,

Table 3 Comparison between experimental data and simulation results for the separation, reattachment location, and maximum Mach number (ONERA case C)

Model	Separation point	Reattachment point	Maximum Mach number
NK	0.291	0.318	1.36
SST	0.264	0.327	1.36
NL k–ϵ	0.256	0.328	1.37
NL k–ϵ–A_2	0.258	0.330	1.39
Experimental[5]	0.260	0.325	1.4

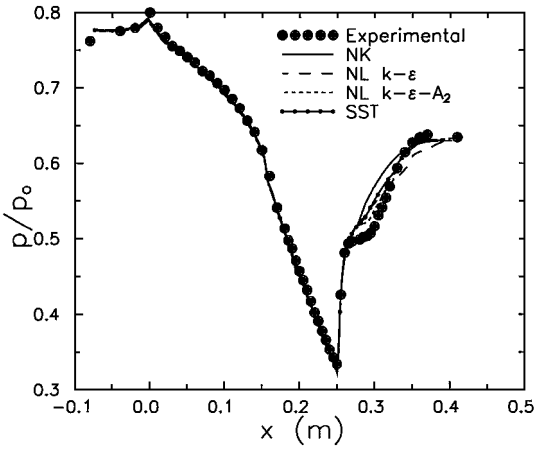

Fig. 5 Comparison between experimental data and numerical results for the surface pressure distribution along the lower wall (ONERA case C).

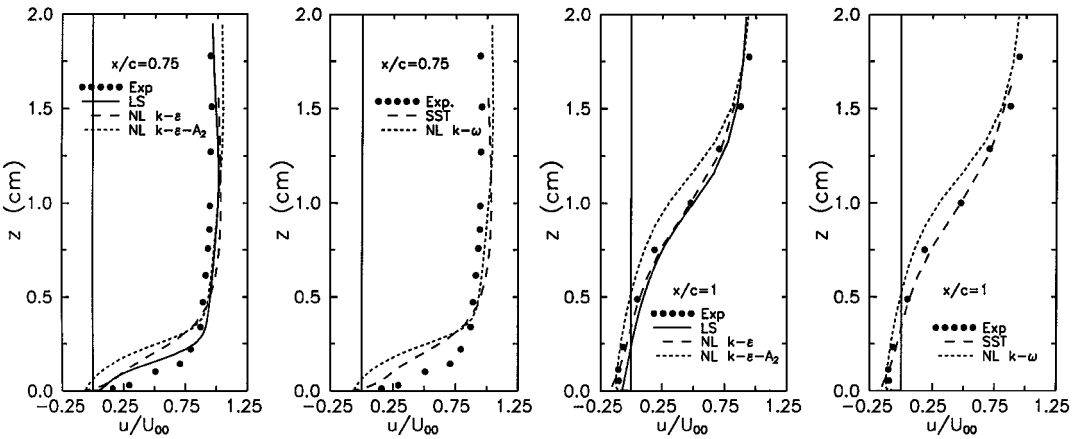

Velocity profiles

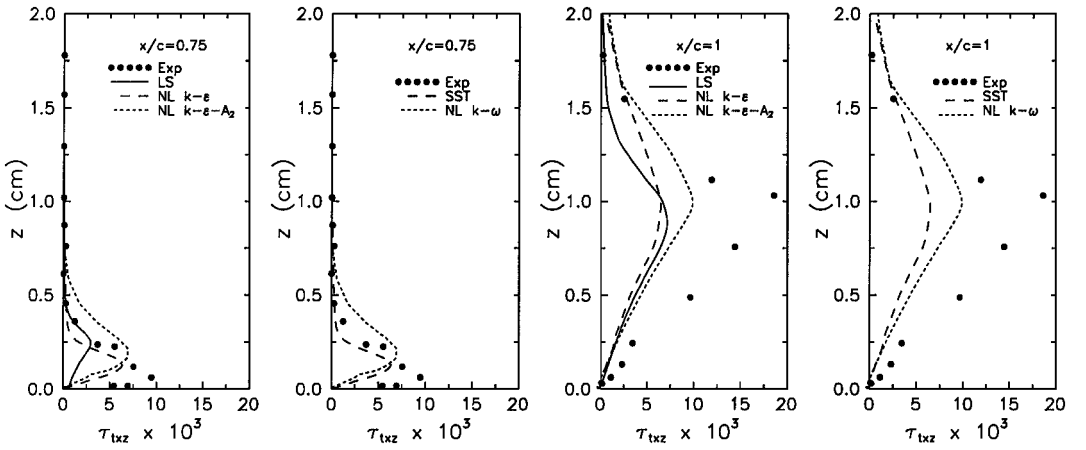

Turbulent shear stress profiles

Fig. 4 Comparison between experimental data and numerical results for the velocity and turbulent shear stress profiles (case 8611) at two locations along the bump.

Table 4 Work units required for computation of the two flow cases[a]

Model	Case 8611	ONERA case C
LS	610	——
NK	——	1090
SST	738	1090
NL k–ϵ	890	1332
NL k–ω	941	——
NL k–ϵ–A_2	1028	1803

[a]A work unit corresponds to a minute of CPU time on a HP 9000/700/99 workstation.

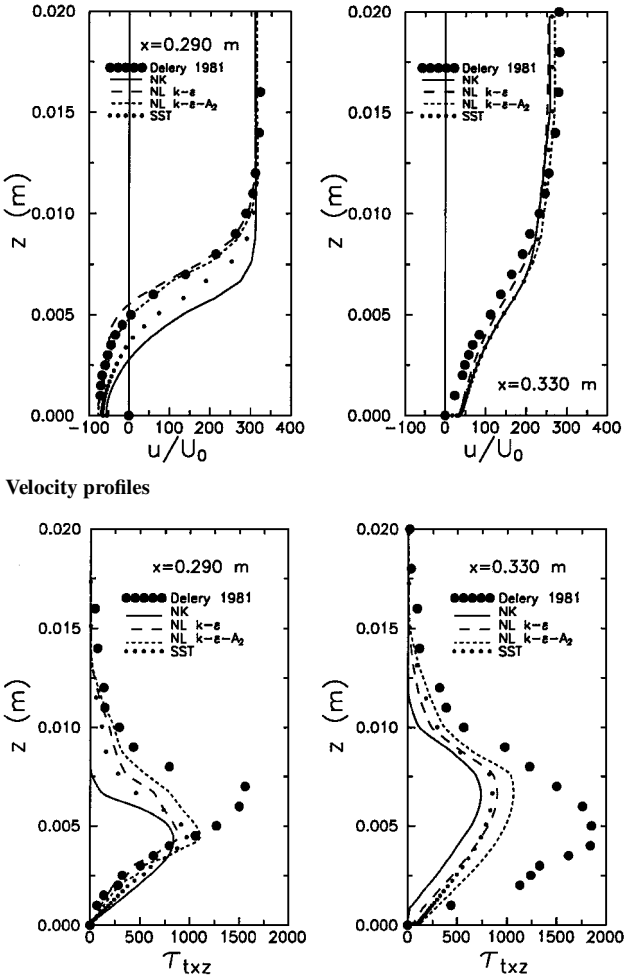

Velocity profiles

Turbulent shear stress profiles

Fig. 6 Comparison between experimental data and numerical results for the velocity and turbulent shear-stress profiles (ONERA case C) at two locations along the bump.

whereas the linear model seems to diffuse the second shock of the λ structure.

Concerning the CPU resources, the nonlinear three-equation model is the most expensive one (Table 4). This is not mainly because of the extra time required for solving the third equation for A_2 quantity but is because this model increases the stiffness of the numerical solution and results, in general, in slower convergence rates. Yet the nonlinear k–ω model also requires longer computing times than the corresponding nonlinear k–ϵ model, at least for the case 8611. Concerning the linear models, the SST k–ω model is, in general, slightly more CPU demanding compared to the linear k–ϵ model. However, the SST k–ω can be used in conjunction with coarser grids in the near-wall region—with values of $y^+ \sim 2$ at the first grid point off the wall—without at the same time deteriorating the grid-independent results. On the other hand, the k–ϵ-based models, both linear and nonlinear, were able to converge only for y^+ values less than 2 for the first grid point off the wall.

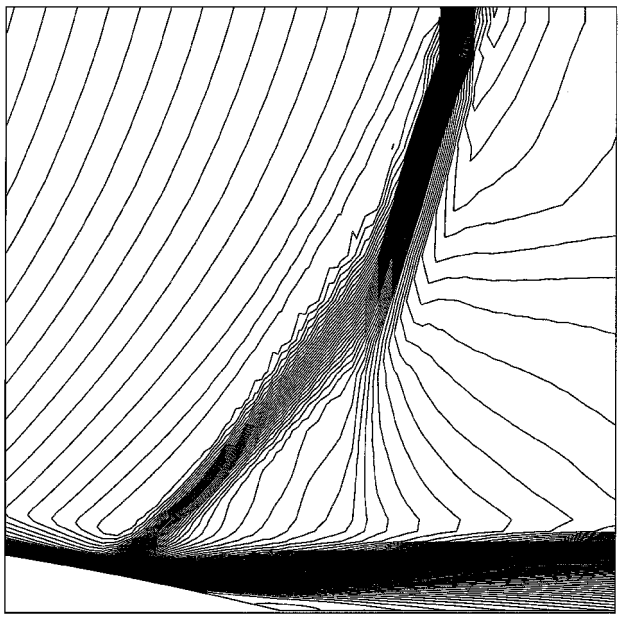

Fig. 7 Prediction of the λ-shock structure using the Nagano–Kim k–ϵ model (ONERA case C).

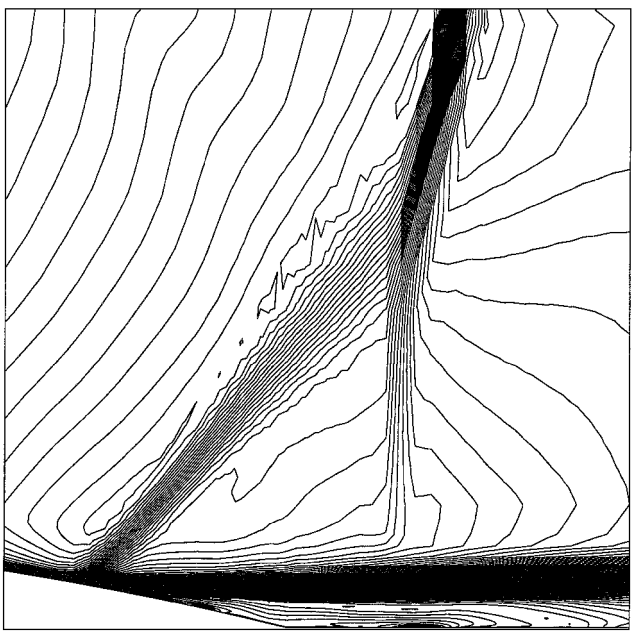

Fig. 8 Prediction of the λ-shock structure using the nonlinear k–ϵ–A_2 model (ONERA case C).

V. Conclusions

This paper presented validation and assessment of several linear and nonlinear k–ϵ and k–ω models in transonic flows over bump geometries, featuring shock/boundary-layer interaction and separation.

A general observation is that although some of the comparisons indicate some improvement of the numerical predictions because of the implementation of nonlinear models other comparisons seem to be inconclusive. Another observation is that all linear k–ϵ models employed here gave worse results than the linear SST k–ω and the nonlinear models. Moreover, the results showed that the SST k–ω model provides in many cases results comparable to the ones obtained by nonlinear models.

The improvement of the results using nonlinear models is evident, especially inside the separation flow region. The nonlinear models improve considerably the prediction of the maximum value of shear stress, but the results are still far from the experiment. Further comparisons with the experimental data (not presented here)

showed that the anisotropy tensor a_{ij} was also underpredicted. Concerning this point, there is still an uncertainty associated with the real levels of turbulence anisotropy appearing in the flowfield and, more specifically, with the anisotropy induced by the shock wave. If the anisotropy is induced by inherent shock oscillations, as Benay et al.[41] have reported, then the present simulations using nonlinear models could not capture this effect because they have not been performed in a time-accurate fashion.

There were also strong similarities between the predictions of the nonlinear k–ϵ and k–ω models because the nonlinear k–ω formulation employed here was derived by the k–ϵ formulation of Craft et al.[10] and Suga[14] with minimal modifications.[19] The pressure plateau appeared in the separated flow region is, generally, better predicted by the nonlinear models. However, the results obtained by the SST k–ω model are also in good agreement with the experiment, especially for case 8611. Furthermore, any aforementioned improvement obtained by the nonlinear models is achieved against an increase of computing time, especially for the case of the nonlinear k–ϵ–A_2 models. The latter leads to stiffer numerical solutions because of the A_2 equation.

Further improvements of the three-equation model are necessary, especially in connection with the computing time reduction. Such efforts can possibly start by examining the influence of the boundary conditions for the A_2 equation or reformulating the model so that it will use a different parameter to increase its sensitivity to the near-wall turbulence anisotropy. A possible alternative is to use the A equation as suggested by Suga.[35]

Acknowledgments

The financial support provided by the Engineering and Physical Sciences Research Council/Ministry of Defence (GR/L18457) is gratefully acknowledged. G. Barakos would also like to thank the National Technical University of Athens (through the L. Economides scholarship) for additional financial support.

References

[1]Bachalo, W. D., and Johnson, D. A., "An Investigation of Transonic Turbulent Boundary Layer Separation Generated on an Axisymmetric Flow Model," AIAA Paper 79-1479, July 1979.

[2]Johnson, D. A., Horstman, C. C., and Bachalo, W. D., "Comparison Between Experiment and Prediction for a Transonic Turbulent Separated Flow," *AIAA Journal*, Vol. 20, No. 6, 1982, pp. 737–744.

[3]Bachalo, W. D., and Johnson, D. A., "Transonic Turbulent Boundary-Layer Separation on an Axisymmetric Flow Model," *AIAA Journal*, Vol. 24, No. 3, 1986, pp. 437–443.

[4]Délery, J. M., "Experimental Investigation of Turbulence Properties in Transonic Shock/Boundary-Layer Interactions," *AIAA Journal*, Vol. 21, No. 2, 1983, pp. 180–185.

[5]Délery, J. M., "Shock Wave/Boundary Layer Interaction and Its Control," *Progress in Aeronautical Sciences*, Vol. 22, No. 4, 1985, pp. 209–280.

[6]Baldwin, B. S., and Lomax, H., "Thin Layer Approximation and Algebraic Model for Separated Turbulent Flows," AIAA Paper 78-257, Jan. 1978.

[7]Gerolymos, G. A., and Vallet, I., "Near-Wall Reynolds-Stress Three-Dimensional Transonic Flow Computations," *AIAA Journal*, Vol. 35, No. 2, 1997, pp. 228–236.

[8]Davidson, L., "Reynolds Stress Transport Modelling of Shock-Induced Separated Flow," *Computers and Fluids*, Vol. 24, No. 3, 1995, pp. 253–268.

[9]Craft, T. J., Launder, B. E., and Suga, K., "A Non-Linear Eddy-Viscosity Model Including Sensitivity to Stress Anisotropy," *Proceedings of the 10th Symposium on Turbulent and Shear Flows*, Vol. 2, 1995, pp. 23-19–23-24.

[10]Craft, T. J., Launder, B. E., and Suga, K., "Development and Application of a Cubic Eddy-Viscosity Model of Turbulence," *International Journal of Heat Fluid Flow*, Vol. 17, No. 2, 1996, pp. 108–115.

[11]Apsley, D. D., and Leschziner, M. A., "A New Low-Re Non-Linear Two-Equation Turbulence Model for Complex Flows," *International Journal of Heat and Fluid Flow*, Vol. 19, No. 3, 1998, pp. 209–222.

[12]Gatski, T. R., "Prediction of Airfoil Characteristics with High Order Turbulence Models," NASA TM-110246, April 1996.

[13]Barakos, G., and Drikakis, D., "Validation of Linear and Non-Linear Low-Re Turbulence Models in Shock/Boundary Layer Interaction," *Proceedings of the 11th Symposium on Turbulent and Shear Flows*, Vol. 3, 1997, pp. 32-19–32-24.

[14]Suga, K., "Development and Application of a Non-Linear Eddy Viscosity Model Sensitized to Stress and Strain Invariants," Ph.D. Dissertation, Dept. of Mechanical Engineering, Thermo-Fluids Div., UMIST, Manchester, England, U.K., 1995.

[15]Launder, B. E., and Sharma, B. I., "Application of the Energy-Dissipation Model of Turbulence to the Calculation of Flow Near a Spinning Disk," *Letters in Heat and Mass Transfer*, Vol. 1, 1974, pp. 131–138.

[16]Nagano, Y., and Kim, C., "A Two-Equation Model for Heat Transport in Wall Turbulent Shear Flows," *Journal of Heat Transfer*, Vol. 110, No. 3, 1988, pp. 583–589.

[17]Menter, F. R., and Rumsey, L. C., "Assessment of Two-Equation Turbulence Models for Transonic Flows," AIAA Paper 94-2343, June 1994.

[18]Menter, F. R., "Two-Equation Eddy-Viscosity Turbulence Models for Engineering Applications," *AIAA Journal*, Vol. 32, No. 8, 1994, pp. 57–63.

[19]Sofialidis, D., and Prinos, P., "Development of a Non-Linear Strain-Sensitive k–ω Turbulence Model," *Proceedings of the 11th Symposium on Turbulent and Shear Flows*, Vol. 2, 1997, pp. 2-89–2-94.

[20]Peyret, R., and Viviand, H., "Computation of Viscous Compressible Flows Based on the Navier–Stokes Equations," AG-212, AGARD, 1975.

[21]Barakos, G., and Drikakis, D., "Implicit-Coupled Implementation of Two-Equation Turbulence Models in Compressible Navier–Stokes Methods," *International Journal for Numerical Methods in Fluids*, Vol. 28, No. 1, 1998, pp. 73–94.

[22]Eberle, A., "Characteristic Flux Averaging Approach to the Solution of Euler's Equations," *VKI Lecture Series in Computational Fluid Dynamics*, No. 1987-04, 1987.

[23]Eberle, A., Rizzi, A., and Hirschel, E. H., "Numerical Solutions of the Euler Equations for Steady Flow Problems," *Notes on Numerical Fluid Mechanics*, Vol. 34, Vieweg, Brunswick, Germany, 1992.

[24]Drikakis, D., and Durst, F., "Investigation of Flux Formulae in Transonic Shock Wave/Turbulent Boundary Layer Interaction," *International Journal for Numerical Methods in Fluids*, Vol. 18, No. 4, 1994, pp. 385–413.

[25]Pope, S. B., "A More General Effective-Viscosity Hypothesis," *Journal of Fluid Mechanics*, Vol. 72, Pt. 2, 1975, pp. 331–340.

[26]Speziale, C. G., "On Nonlinear K–l and K–ϵ Models of Turbulence," *Journal of Fluid Mechanics*, Vol. 178, 1987, pp. 459–475.

[27]Speziale, C. G., and Ngo, T., "Numerical Solution of Turbulent Flow Past a Backward-Facing Step Using a Non-Linear k–ϵ Model," *International Journal of Engineering Science*, Vol. 26, No. 10, 1988, pp. 1099–1112.

[28]Rubinstein, R., and Barton, J. M., "Nonlinear Reynolds Stress Models and the Renormalization Group," *Physics of Fluids A*, Vol. 2, No. 8, 1990, pp. 1472–1476.

[29]Yakhot, V., and Orszag, S. A., "Renormalization Group Analysis of Turbulence: I. Basic Theory," *Journal of Scientific Computing*, Vol. 1, No. 1, 1986, pp. 3–51.

[30]Orszag, S. A., Yakhot, V., Flannery, W. S., and Boysan, F., "Renormalization Group Modelling and Turbulence Simulations," *Near Wall Turbulent Flows*, edited by R. M. So and C. G. Speziale, Elsevier, Amsterdam, 1993, pp. 155–183.

[31]Shih, T.-H., Zhu, J., and Lumley, J. L., "A Realizable Reynolds Stress Algebraic Equation Model," NASA TM-105993, Jan. 1993.

[32]Jiang, Y. T., Damodaran, M., and Lee, K. H., "High-Resolution Finite Volume Computation of Turbulent Transonic Flow Past Airfoil," *AIAA Journal*, Vol. 35, No. 7, 1997, pp. 1134–1142.

[33]Lien, F.-S., and Leschziner, M. A., "Modelling 2D Separation from a High Lift Aerofoil with a Non-Linear Eddy-Viscosity Model and Second-Moment Closure," *Aeronautical Journal*, Vol. 99, No. 984, 1995, pp. 125–144.

[34]Liou, W. W., and Shih, T. H., "Transonic Turbulent Flow Predictions with Two-Equation Turbulence Models," NASA CR-198444, Jan. 1996.

[35]Suga, K., "Nonlinear Eddy Viscosity Modelling with a Transport Equation for Lumley's Stress Flatness Parameter," *Proceedings of the 11th Symposium on Turbulent and Shear Flows*, Vol. 1, 1997, pp. 13-18–13-23.

[36]Haase, W., Brandsma, F., Elsholz, E., Leschziner, M., and Schwambron, D. (eds.), *EUROVAL, A European Initiative on Validation of CFD Codes*, Vol. 42, Notes on Numerical Fluid Mechanics, Vieweg, Brunswick, Germany, 1993.

[37]Kline, S. J., Cantwell, B. J., and Lilley, G. M. (eds.), "1980–81 AFOSR–HTTM–Stanford Conference on Complex Turbulent Flows," Thermo-Sciences Div., Stanford Univ., Stanford, CA, 1981.

[38]Barakos, G., and Drikakis, D., "Assesment of Various Low-Re Turbulence Models in Shock/Boundary Layer Interaction," *Computer Methods in Applied Mechanics and Engineering*, Vol. 160, Nos. 1–2, 1998, pp. 155–174.

[39]Marvin, J. G., and Huang, G. P., "Turbulence Modeling—Progress and Future Outlook," *15th International Conference on Numerical Methods in Fluid Dynamics*, 1996.

[40]Bardina, J. E., Huang, P. G., and Coakley, T. J., "Turbulence Modeling Validation, Testing, and Development," NASA TM-110446, April 1997.

[41]Benay, R., Cöet, C., and Délery, J., "A Study of Turbulence Modelling in Transonic Shock-Wave Boundary-Layer Interactions," *Turbulent Shear Flows 6: Selected Papers from the 6th International Symposium on Turbulent and Shear Flows*, 1st ed., Vol. 6, Springer–Verlag, Berlin, 1989, pp. 194–205.

C. G. Speziale
Associate Editor